# Detection and Identification of a Chromophoric Intermediate during the Medium-Chain Fatty Acyl-CoA Dehydrogenase-Catalyzed Reaction via Rapid-Scanning UV/Visible Spectroscopy†

Jeffrey K. Johnson and D. K. Srivastava*

*Biochemistry Department, North Dakota State University, Fargo, North Dakota 58105*

*Received March 4, 1993; Revised Manuscript Received April 30, 1993*

ABSTRACT: We have investigated the medium-chain fatty acyl-CoA dehydrogenase (MCAD)- catalyzed reaction via rapid-scanning stopped-flow (RSSF) UV/vis spectroscopy, combined with the single-wavelength stopped-flow technique, utilizing 3-indolepropionyl-CoA (IPCoA) and *trans*-3-indoleacryloyl-CoA (IACoA) as chromophoric pseudosubstrates. The RSSF spectral data reveal that formation of an intermediary species with an absorbance maximum at 400 nm and a broad charge-transfer band around 600 nm accompanies the reduction of MCAD–FAD by IPCoA. In the presence of high concentrations of enzyme ([MCAD] >> [IPCoA]) the intermediary spectral band at 400 nm remains unperturbed, whereas in the presence of low concentrations of enzyme ([MCAD] << [IPCoA]) it slowly shifts to an absorption band with an absorbance maximum at 370 nm. Appearance and disappearance of this intermediary species coincides with the appearance and disappearance of the charge-transfer band. Single-wavelength stopped-flow studies, performed under similar high and low enzyme conditions, were consistent with one ($1/\tau_1$) and two ($1/\tau_1 > 1/\tau_2$) relaxation rate constants, respectively. These findings, combined with relaxation studies performed in the reverse directions as well as substrate and product binding studies with the oxidized and reduced forms of the enzyme, have allowed us to conclude the following: (1) the intermediary species possesses the properties of reduced flavin and highly conjugated reaction product IACoA (absorbance maximum = 400 nm); (2) this intermediary species collapses into an MCAD–$FADH_2$–IACoA complex (absorbance maximum = 370 nm) in the presence of excessive concentrations of IPCoA; the collapse is being driven by the competitive binding of IPCoA with the reduced form of the enzyme; (3) the 400-nm absorption band and the charge-transfer band are given by the same intermediary species formed during the enzyme-catalyzed reaction pathway. The role of protein conformational changes in modulating the substrate/product structures during the MCAD-catalyzed reaction is discussed.

## INTRODUCTION

Medium-chain fatty acyl-CoA dehydrogenase (MCAD)[1] catalyzes the first step in the $\beta$-oxidation of fatty acids (Beinert, 1963). The enzyme-catalyzed reaction proceeds via a concerted abstraction of a proton and a hydride ion from the $\alpha$- and $\beta$-carbons of fatty acyl-CoA chains, respectively, concomitant with the reduction of the MCAD-bound FAD to $FADH_2$ (Ghisla et al., 1984; Pohl et al., 1986; Schopfer et al., 1988). The repetitive turnover of the enzyme is maintained (under physiological conditions) by transfer of electrons from MCAD–$FADH_2$ to the electron-transferring flavoprotein ETF–FAD (Crane & Beinert, 1956). MCAD utilizes a broad range of aliphatic ($C_4$–$C_{16}$) (Crane et al., 1956; Thorpe et al., 1979) and aromatic/heterocyclic ring-substituted pseudosubstrates, such as furylpropionyl-CoA, phenylpropionyl-CoA, and hydrocinnamoyl-CoA (McFarland et al., 1982; Knoop, 1904; Murfin, 1974). Recently, we demonstrated that 3-indolepropionyl-CoA (IPCoA) serves as a competent substrate for this enzyme (eq 1) and that the reaction product, *trans*-3-indoleacryloyl-CoA (IACoA), serves as an excellent

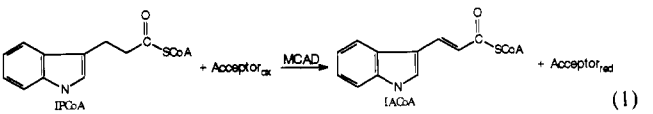

(1)

chromophoric probe (absorbance maximum = 367 nm, $\epsilon_{367}$ = 26 500 $M^{-1}$ $cm^{-1}$) for investigating some mechanistic details of the MCAD-catalyzed reaction (Johnson et al., 1992).

Due to the chromophoric nature of IACoA, we could directly monitor the enzyme-catalyzed oxidation of IPCoA without recourse to signals associated with the "colored" electron acceptors (such as DCPIP, $FcPF_6$, etc.) (Lehman et al., 1990). In this way, we discerned that the MCAD-catalyzed oxidation of IPCoA proceeds via dehydrogenase (in the presence of "organic" electron acceptors) as well as via oxidase (in which oxygen acts as the electron acceptor) pathways, and we determined the steady-state kinetic parameters of this enzyme under these pathways. The chromophoric potential of IACoA also allowed us to probe the microscopic environment of the enzyme site under different redox states of the enzyme. We observed that the electronic spectrum of IACoA is red-shifted upon interaction with both the FAD and $FADH_2$ forms of the enzyme (Johnson et al., 1992). On the contrary, the spectrum of the enzyme-bound FAD is blue-shifted with marked resolutions of the vibrational structures (Auer & Frerman, 1980). These observations, coupled with the transient kinetic analysis for the interaction of MCAD–FAD with IACoA and pH jump studies, allowed us to delineate the pathway by which MCAD–FAD–IACoA isomerization (via protein conforma-

† Journal article 2099 of the North Dakota Agricultural Experiment Station. Supported by the American Heart Association, Dakota Affiliate.

* To whom correspondence should be addressed.

[1] Abbreviations: MCAD, medium-chain fatty acyl-CoA dehydrogenase; IPCoA, 3-indolepropionyl coenzyme A; IACoA, *trans*-3-indoleacryloyl coenzyme A; $FcPF_6$, ferricinium hexafluorophosphate; FAD, flavin adenine dinucleotide; $FADH_2$, reduced flavin adenine dinucleotide; EDTA, ethylenediaminetetraacetic acid; RSSF rapid-scanning stopped-flow spectroscopy.

0006-2960/93/0432-8004$04.00/0 

tional changes) is coupled to the proton equilibration steps between the two alternative forms of the enzyme (Johnson et al., 1992).

These studies prompted us to elaborate on the roles of the enzyme site environment in modulating the substrate/product structure, and vice versa, during the course of MCAD catalysis. To achieve this goal, we decided to monitor the spectral changes of both flavin and indole chromophoric species during the course of the MCAD-catalyzed reaction. These studies were facilitated by the use of the repetitive rapid-scanning stopped-flow (RSSF) technique. As will be shown subsequently, the use of the chromophoric pseudosubstrate and the RSSF technique has uniquely enabled us to detect and characterize an intermediary species which is formed during the course of the enzyme-catalyzed reaction.

## MATERIALS AND METHODS

*Materials.* Coenzyme A, glucose oxidase (type VII), and EDTA were purchased from Sigma. 3-Indolepropionic acid and *trans*-3-indoleacrylic acid, used in the synthesis of substrates, were purchased from Aldrich. All other reagents were of analytical grade.

*Methods.* The CoA derivatives of 3-indolepropionic acid (IPCoA) and *trans*-3-indoleacrylic acid (IACoA) were synthesized and purified according to the procedures described previously (Johnson et al., 1992). Medium-chain fatty acyl-CoA dehydrogenase (MCAD) was purified in our laboratory as described previously (Johnson et al., 1992).

All experiments were performed in a standard 50 mM potassium phosphate buffer pH 7.6 containing 0.3 mM EDTA at 25 °C unless stated otherwise. MCAD was routinely assayed in this buffer utilizing 30 μM octanoyl-CoA and 200 μM ferricinium hexafluorophosphate ($FcPF_6$) as described by Lehman et al. (1990). The active enzyme concentration was determined in terms of the flavin content by using an extinction coefficient of 15.4 $mM^{-1}$ $cm^{-1}$ at 446 nm (Thorpe et al., 1979). IPCoA and IACoA concentrations were determined using extinction coefficients of 18.2 $mM^{-1}$ $cm^{-1}$ at 259 nm and 26.5 $mM^{-1}$ $cm^{-1}$ at 367 nm, respectively (Johnson et al., 1992).

Steady-state kinetics and conventional spectral acquisitions were performed on a Perkin-Elmer Lambda 3B spectrophotometer. Circular dichroic spectral acquisition and titration experiments were performed on a Jasco J700 spectropolarimeter. Single-wavelength transient kinetic studies and data analyses were performed on an Applied Photophysics MV-14 stopped-flow system.

*Rapid-Scanning Stopped-Flow (RSSF) Spectrophotometry.* The RSSF spectrophotometer used in these studies was configured similarly to the system utilized by Dunn and collaborators (Koerber et al., 1983). Our system employed the elements of a Durrum stopped-flow, Jarrell Ash type 1208 polychromator, a Model 1410 Princeton Applied Research diode array, and a Model 1215 Princeton Applied Research OMA-2 multichannel analyzer. An external time-delay firing circuit was used to trigger the stopped-flow and initiate data acquisition such that flow cessation and data collection would occur at approximately the same time. Full spectral output from xenon or tungsten source lamps, for studies in the 345–490- or 400–540-nm ranges, respectively, was used to illuminate the stopped-flow cuvette. Spectral traces were smoothed using the method of Savitsky and Golay (1964).

*Dissociation Constant of the MCAD–$FADH_2$–IPCoA Complex.* The dissociation constant of the reduced MCAD–IPCoA complex was determined by CD spectroscopy utilizing a procedure developed in our laboratory (Wang et al., 1992). A 1.65-mL volume of 25 μM MCAD was reduced with a 10-fold excess of sodium dithionite under anaerobic conditions. This solution was then titrated by addition of known volumes of a 0.2 mM IPCoA solution, and the difference in ellipticity was measured at 420 nm.

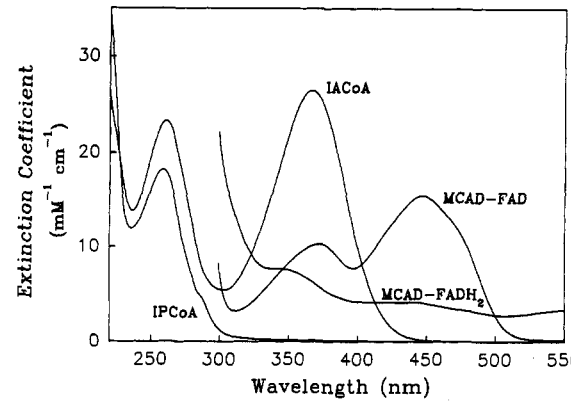


FIGURE 1: UV/vis spectra of IPCoA, IACoA, MCAD–FAD, and MCAD–$FADH_2$ in 50 mM potassium phosphate buffer pH 7.6 containing 0.3 mM EDTA at 25 °C. Spectra are plotted as extinction coefficient versus wavelength.

*Anaerobic Experiments.* Buffers and solutions were made anaerobic by bubbling and degassing in 2–15-min cycles with argon scrubbed free of oxygen using an oxytrap (Alltech). Immediately prior to using these reagents in the rapid-scan or stopped-flow systems, we added glucose oxidase and glucose to concentrations of 30 μg/mL and 0.8 mM, respectively, to remove any traces of oxygen.

*Computer Simulations.* Simulation of the MCAD mechanism described in this paper was performed using the program PLOD of D. K. Kahaner and D. D. Barnet (Center for Computing and Applied Mathematics, National Institute of Standards and Technology, Gaithersburg, MD 20899) as described by Betts and Srivastava (1991).

## RESULTS

Figure 1 shows the UV/vis absorption spectra of the oxidized and reduced forms of the (enzyme-bound) flavin and acyl-CoA (indolepropionyl-CoA and indoleacryloyl-CoA) pseudosubstrates. Note that both the flavin and acyl-CoA pseudosubstrate give pronounced visible spectra in their oxidized states as compared to their respective reduced forms. Hence, during enzyme-catalyzed oxidation/reduction reactions, the absorption bands of the oxidized flavin (MCAD–FAD) are expected to diminish at both the 370- and 450-nm regions, whereas the absorption band due to formation of IACoA is expected to increase at 367 nm. Given the nature of spectral transitions of flavin and acyl-CoA chromophores, we decided to investigate the transient courses of the MCAD–FAD + IPCoA → and the MCAD–$FADH_2$ + IACoA → reactions via rapid-scanning stopped-flow (RSSF) and single-wavelength stopped-flow techniques.

*Transient Kinetic Studies of the Reduction of MCAD–FAD by IPCoA under Conditions Where [MCAD–FAD] >> [IPCoA].* Figure 2 shows the RSSF spectral data for the enzyme/substrate reaction in two separate regions, i.e., between 360 and 480 nm (Figure 2A) and between 408 and 535 nm (Figure 2C), upon mixing 60 μM MCAD–FAD with 12 μM IPCoA in the stopped-flow syringes. It was necessary to perform two separate spectral acquisition experiments because of the limitation in the physical assembly of our polychromator and diode array detector. In each of these

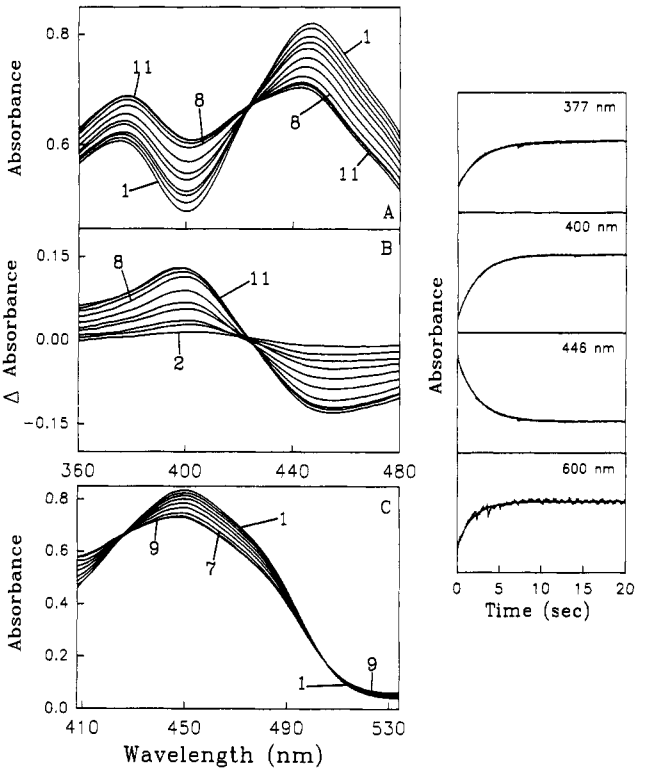


FIGURE 2: Rapid-scanning stopped-flow spectra for the reduction of MCAD-FAD by IPCoA under anaerobic conditions, where [MCAD-FAD] >> [IPCoA]. Spectra in panels A and C represent the time courses for the reaction of 60 μM MCAD–FAD and 12 μM IPCoA. Other conditions are the same as in Figure 1. Spectra in panel B represent the difference spectra (i.e., the spectra at a given time minus the first spectrum) derived from the data of panel A. The time sequence for traces in panels A and C are as follows: panel A, traces 2–11, (2) 0.22, (3) 0.48, (4) 0.65, (5) 1.08, (6) 1.51, (7) 2.37, (8) 4.1, (9) 9.3, (10) 17.0, and (11) 24.7 s; panel C, traces 2–9, (2) 0.22, (3) 0.48, (4) 0.89, (5) 1.51, (6) 2.37, (7) 4.1, (8) 9.3, and (9) 24.7 s. Panels on the right represent single-wavelength stopped-flow traces obtained upon mixing 50 μM MCAD–FAD and 10 μM IPCoA. The rate constants calculated from these traces are 0.35, 0.43, 0.43, and 0.53 $s^{-1}$ at 377, 400, 446, and 600 nm, respectively.

spectral regions, the first spectrum has been obtained within 2 ms after the mixing of the reactants. Note that the first spectrum in Figure 2A is characterized by the presence of two pronounced absorption peaks, at 370 and 450 nm, indicative of the oxidized flavin chromophore. An exactly similar spectrum (zero-time spectrum) can be reconstituted by summation of the individual spectra of MCAD–FAD and IPCoA, obtained upon the mixing of the individual species against buffer in the stopped-flow syringes under identical experimental conditions (data not shown). This implies that no spectral changes took place within the dead time (3–5 ms) of our stopped flow.

Spectra 2–11 of Figure 2A and C represent the time-resolved spectra of the MCAD–FAD and IPCoA reaction ([MCAD-FAD] >> [IPCoA]) up to 25 s. Due to slow bleaching of the flavin chromophore under irradiation by the high-intensity xenon lamp (particularly under anaerobic conditions) used in our RSSF system, we could not collect reliable spectra at high enzyme concentrations for times longer than 25 s. However, in this time region (i.e., 25 s) the reaction has reached completion, as confirmed by single-wavelength stopped-flow studies (see below). From the spectral data of Figure 2, it is evident that the reaction progress is accompanied by bleaching of the flavin absorption band between 423 and 507 nm, with concomitant increases in absorption (between 360 and 423 nm and above 507 nm) due to the formation of IACoA and the charge-transfer band, respectively. The time-resolved spectral changes between 360 and 535 nm are consistent with two isosbestic points at 423 and 507 nm, respectively, suggesting a one-step transition between chromophoric species (see below and Discussion). However, the isosbestic point at 423 nm is not as clear in Figure 2A as in Figure 2C due to some bleaching effect of the oxidized flavin under the high irradiation source of the xenon lamp (used at the lower wavelength region); such an effect is clearly absent when a tungsten lamp is used to acquire higher wavelength spectra (as in Figure 2C).

Figure 2B shows the difference spectra, i.e., the spectra at a given time minus the first spectrum (generated from the data of Figure 2A), for the MCAD–FAD + IPCoA reaction. The most noteworthy spectral feature of these data is the appearance of a new spectral band centered at 400 nm, a region where neither the MCAD–FAD nor the IACoA chromophoric species contributes substantially. This 400-nm band attains a maximum within 10 s and remains stable under the experimental conditions employed (i.e., [MCAD-FAD] >> [IPCoA]). This 400-nm band is stable for much longer periods of time (up to 200 seconds) under experimental conditions identical to those employed during the RSSF experiments, as determined using single-wavelength stopped-flow spectroscopy (data not shown). In addition to these spectral changes, the reaction progress was accompanied also by an emergence of a broad charge-transfer band around 507–800 nm (data not shown). Such charge-transfer bands are the ubiquitous property of the MCAD-catalyzed reaction, irrespective of the type of the substrate (albeit with slightly different absorption maxima) (Murfin, 1974; Reinsch et al., 1980). The origin of the charge-transfer complex is attributed to the partial transfer of electrons from reduced flavin to the oxidized substrate within the enzyme phase (Engel, 1992).

Although in principle the RSSF spectral data can be directly transformed into time-dependent absorption changes at different wavelengths, such strategies are known to preclude quantitative assessments of the number of relaxation steps during the course of reaction. With this limitation in mind, we performed single-wavelength stopped-flow relaxation studies under experimental conditions identical to those of Figure 2A and C. These stopped-flow kinetic traces at selected wavelengths are shown in the right-hand panels in Figure 2. The kinetic traces (increasing or decreasing) are consistent with a single-step relaxation process with an average $1/\tau = 0.44 \pm 0.07\ s^{-1}$. To ascertain whether the observed relaxation involves a one- or two-step equilibration process, we measured the enzyme concentration-dependent relaxation rate constant at several wavelengths under pseudo-first-order conditions for the enzyme ([MCAD–FAD] >> [IPCoA]). The observed relaxation rate constant shows a hyperbolic dependence on the enzyme concentration (Figure 3), with $1/\tau_{(max)}$, $1/\tau_{(min)}$, and the MCAD–FAD concentration required to attain the half-saturation ($K_{0.5}$) to be 0.7 $s^{-1}$, 0.08 $s^{-1}$, and 14 μM, respectively.

We were initially surprised by the observation that the spectral band formed at 400 nm is stable (see Figure 2B) at high enzyme concentrations ([MCAD–FAD] >> [IPCoA]). This is because no spectral band of this type was detected in our earlier experiments when we attempted to investigate the influence of the enzyme site (MCAD–$FADH_2$) environment on the electronic structure of IACoA (Johnson et al., 1992). For example, when we incubated 10 μM MCAD–FAD with 16 μM IACoA, the resultant (static) spectrum showed an absorption maximum at 373 nm (Johnson et al., 1992). This

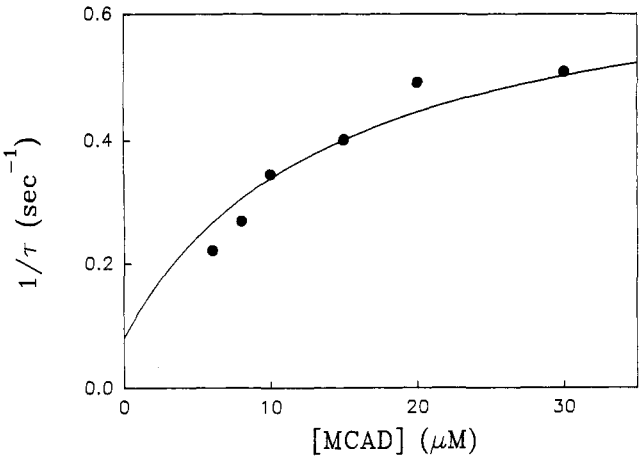


FIGURE 3: MCAD–FAD concentration-dependent relaxation rate constants for the reaction of MCAD–FAD with IPCoA measured at 400 nm. The IPCoA concentration after mixing was 1 $\mu$M. The MCAD–FAD concentration on the $x$-axis also represents the concentration of the enzyme after mixing. Other conditions are the same as in Figure 2. The solid line has been calculated for a hyperbolic dependence (with offset) of $1/\tau$ as a function of MCAD–FAD concentration, with $1/\tau_{(max)} = 0.7$ s$^{-1}$, $1/\tau_{(min)} = 0.08$ s$^{-1}$, and $K_{0.5} = 14$ $\mu$M.

absorbance maximun was further blue-shifted when the incubation mixture contained a higher concentration of IPCoA. This led us to suspect that the higher concentration of IPCoA might be responsible for the displacement of IACoA (which is red-shifted) from the active site of the enzyme (see Discussion).

*Transient Kinetic Studies of the Reduction of MCAD–FAD by IPCoA under Conditions Where [IPCoA] >> [MCAD–FAD].* Figure 4 shows the time-resolved spectra upon the mixing of 20 $\mu$M MCAD–FAD with 200 $\mu$M IPCoA in the stopped-flow syringes. From a comparison of these spectra with those of Figure 2 (where [MCAD–FAD]>> [IPCoA]), two interesting features are noteworthy. (1) The spectral band centered at 400 nm (Figure 2) is not stable but is "transient" in nature, as it undergoes a slow blue shift to 370 nm. Since all the experiments reported herein have been performed under anaerobic conditions, this spectral transition is not caused by a repetitive oxidative turnover of the enzyme. (2) No clean isosbestic points are observed during the time-dependent spectral transitions. Both of these spectral properties suggest that more than two (spectrally distinct) species are generated under these experimental conditions (i.e., when [MCAD–FAD] << [IPCoA]) and that the transient species observed at 400 nm is an intermediate (X) in the reaction pathway (see Scheme I). It is important to note that the time course of this reaction occurs over approximately a 4-min period, in which the intermediate X reaches a maximum in approximately 5 s and then begins to decay (see single-wavelength stopped traces of Figure 4).

In addition to the RSSF data between 350 and 535 nm, we also collected time-resolved spectra in the charge-transfer region (data not shown). Under the present experimental conditions, there was an initial buildup of the charge-transfer complex band (with an absorption maximum around 600 nm), followed by a slow diminution of this band. As shown in Figure 4C, the increase and decrease in absorption in the charge-transfer region (partially shown between 507 and 535 nm) coincide with the appearance and disappearance of the 400-nm intermediary species X. Single-wavelength stopped-flow traces at 400 and 600 nm show this correlation more effectively (see accompanying right-hand panels of Figure 4).

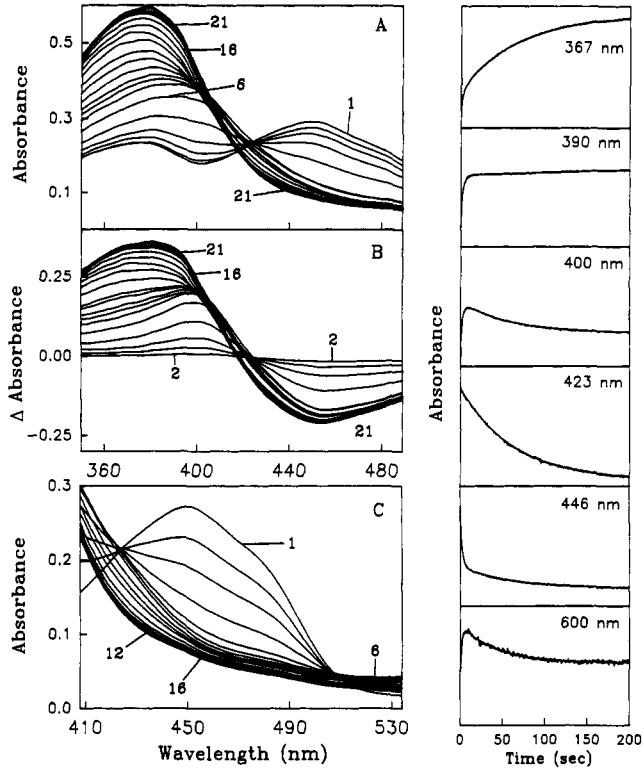


FIGURE 4: Rapid-scanning stopped-flow spectra for the reduction of MCAD–FAD by IPCoA under anaerobic conditions, where [IPCoA] >> [MCAD–FAD]. Spectra in panels A and C are time-dependent spectra observed upon the mixing of 20 $\mu$M MCAD–FAD with 200 $\mu$M IPCoA in the stopped-flow syringes. Spectra in panel B represent the difference spectra derived from the data of panel A. Other conditions are the same as in Figure 2. The time sequence for the traces in panels A and C are as follows: panel A, traces 2–21, (2) 0.138, (3) 0.31, (4) 0.65, (5) 1.51, (6) 4.1, (7) 6.28, (8) 10.1, (9) 11.9, (10) 17.0, (11) 24.7, (12) 34.3, (13) 51.4, (14) 68.6, (15) 103, (16) 137, (17) 172, (18) 206, (19) 241, (20) 258, and (21) 275 s; panel C, traces 2–16, (2) 0.65, (3) 1.51, (4) 3.24, (5) 6.7, (6) 10.1, (7) 17.0, (8) 34.2, (9) 51.4, (10) 68.6, (11) 103, (12) 137, (13) 172, (14) 206, (15) 241, and (16) 282 s. Panels on the right represent single-wavelength stopped-flow traces for the reaction of 10 $\mu$M MCAD–FAD with 200 $\mu$M IPCoA. The rate constants calculated from these traces are, for 367 nm, $1/\tau_1 = 0.39$ s$^{-1}$, $1/\tau_2 = 0.014$ s$^{-1}$; for 390 nm, $1/\tau_1 = 0.43$ s$^{-1}$; for 400 nm, $1/\tau_1 = 0.44$ s$^{-1}$, $1/\tau_2 = 0.017$ s$^{-1}$; for 423 nm, $1/\tau_2 = 0.016$ s$^{-1}$; for 446 nm, $1/\tau_1 = 0.48$ s$^{-1}$, $1/\tau_2 = 0.018$ s$^{-1}$; and for 600 nm, $1/\tau_1 = 0.52$ s$^{-1}$, $1/\tau_2 = 0.024$ s$^{-1}$. In some cases, (e.g., at 600 nm) the fit line precisely matches a portion of the experimental stopped-flow trace, thereby masking its appearance.

This suggests that the chemical events underlying the formation of the 400-nm spectral band gives rise to the charge-transfer spectral band (see Discussion).

We performed single-wavelength stopped-flow studies under pseudo-first-order conditions for the substrate (i.e., [IPCoA] >> [MCAD–FAD]) to quantitate the number of relaxation times and ascertain the presence of any isoabsorption points (the wavelength at which the absorbance remains constant, but nonzero, during one or more phases but not during all phases of the reaction (MacGibbon et al., 1987)). As is evident from the data of Figure 4, the absorption changes are either positive (increase), negative (decrease), or a combination of the two. At a majority of the wavelengths, the absorption changes are consistent with two relaxation times, $1/\tau_1 > 1/\tau_2$. However, at certain wavelengths, the absorption changes are isoabsorptive to one or the other relaxation time. For example, at 423 nm the fast relaxation time ($1/\tau_1$) is absent, whereas at wavelength 390 nm, the slow relaxation time ($1/\tau_2$) is absent. Note that $1/\tau_1$ and $1/\tau_2$ vary between 0.39 and 0.52 s$^{-1}$ and between 0.014 and 0.024 s$^{-1}$, respectively. The existence of

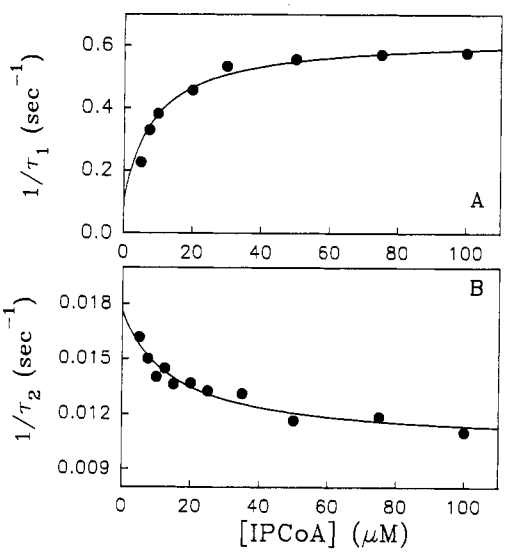


FIGURE 5: IPCoA concentration-dependent relaxation rate constants ($1/\tau_1$ and $1/\tau_2$) for the reaction of MCAD–FAD and IPCoA. In these studies, $1/\tau_1$ (panel A) and $1/\tau_2$ (panel B) have been measured at 400 and 415 nm, respectively. The MCAD–FAD concentration after mixing was 1 $\mu$M. The IPCoA concentration on the $x$-axis represents the concentration after mixing. Other conditions are the same as in Figure 2. The solid lines have been calculated for a hyperbolic dependence (increasing or decreasing, with an offset) of $1/\tau$ values as a function IPCoA concentration. The $1/\tau_{1(max)}$, $1/\tau_{1(min)}$, and $K_{0.5}$ in panel A are 0.63 $s^{-1}$, 0.1 $s^{-1}$, and 9.0 $\mu$M, respectively, whereas the $1/\tau_{2(max)}$, $1/\tau_{2(min)}$, and $K_{0.5}$ in panel B are 0.0176 $s^{-1}$, 0.01 $s^{-1}$, and 14.7 $\mu$M, respectively.

two relaxation times is in accord with the detailed kinetic analysis of Schopfer et al. (1988), in which butyryl-CoA was utilized as the enzyme substrate.

Figure 5 shows the dependence of the $1/\tau$ values on [IPCoA], under conditions where [IPCoA] >> [MCAD–FAD]. Note that while the faster relaxation rate constant ($1/\tau_1$) increases hyperbolically, the slower relaxation rate constant decreases correspondingly as a function of IPCoA concentration. The dependence of $1/\tau_1$ on [IPCoA] is identical to the relationship of $1/\tau$ versus [MCAD–FAD] under opposite experimental conditions (i.e., [MCAD–FAD] >> [IPCoA]). The magnitudes of $1/\tau_{1(max)}$, $1/\tau_{1(min)}$, and $K_{0.5}$ obtained from the best fit of the experimental data (according to the hyperbolic equation with offset) are 0.63 $s^{-1}$, 0.1 $s^{-1}$, and 9.0 $\mu$M, respectively. Note a remarkable similarity between these parameters and those obtained from the data of Figure 3. This, coupled with fact that $1/\tau_1$ is at least 50 times greater than $1/\tau_2$ (at a saturating concentration of IPCoA), suggests (1) that the events occurring during $1/\tau_1$ precede those occurring during $1/\tau_2$ and (2) that both of the relaxation times are not intimately coupled (see Discussion).

Unlike the clear dependence of $1/\tau$ on [MCAD–FAD] (Figure 3) and of $1/\tau_1$ on [IPCoA] (Figure 5), the interpretation of $1/\tau_2$ versus [IPCoA] is not straightforward (see Discussion). A decrease in the slow relaxation rate with increasing substrate concentration has been observed previously in a number of other laboratories (Hall et al., 1979; Reinsch et al., 1980; Pohl et al., 1986; Schopfer et al., 1988). The hyperbolic decrease in $1/\tau_2$ as a function of [IPCoA] clearly suggests that the substrate IPCoA enters into the reaction scheme for a second time, resulting in the disappearance of the intermediate X.

*Transient Kinetic Studies of the Oxidation of MCAD–FADH₂ by IACoA.* Figure 6 shows the RSSF data for the reaction between 20 $\mu$M MCAD–$FADH_2$ and 50 $\mu$M IACoA. Note that the time-resolved spectra obtained in this direction are qualitatively a reverse of those obtained for the reaction of MCAD–FAD with IPCoA (see Figure 4). At initial time regimes, the RSSF spectra shown in Figure 6 are consistent with a single isosbestic point at 395 nm, with a decrease and an increase in absorption below and above this wavelength, respectively. After approximately 5–10 s, this isosbestic point is lost, suggesting more than a one-step transition between the chromophoric species. Unlike the RSSF data for the reaction in the forward direction, a small perturbation in the spectral property of IACoA was observed (within the dead time of the stopped-flow) upon its interaction with MCAD–$FADH_2$. This feature became apparent, as shown in the inset of Figure 6A, upon comparison of the first spectrum with the zero-time spectrum (constructed by summation of the individual spectra). Such perturbation was not unexpected since we had already observed changes in the electronic structure of IACoA upon interaction with the reduced form of the enzyme (Johnson et al., 1992).

Single-wavelength stopped-flow experiments were performed for the oxidation of MCAD–$FADH_2$ with IACoA under a pseudo-first-order condition (i.e., [IACoA] >> [MCAD–$FADH_2$]). In these experiments, MCAD–$FADH_2$ was generated in the presence of a slightly excess molar concentration of sodium dithionite. Note that from the data of Figure 6, the time course of reaction at 377 and 415 nm is clearly biphasic in nature, with relaxation rate constants $1/\tau_1$ (2.1 $s^{-1}$) > $1/\tau_2$ (0.08 $s^{-1}$). We examined the dependence of $1/\tau_1$ and $1/\tau_2$ on IACoA concentration maintaining a pseudo-first-order condition (Figure 7). Note further that while $1/\tau_1$ increases hyperbolically as a function of IACoA, $1/\tau_2$ exhibits practically no dependence (with a maximum variation from 0.05 to 0.1 $s^{-1}$) on IACoA concentration (see Discussion). It is interesting to note that the magnitude of $1/\tau_2$ is approximately equal to $k_{-1}$ (of Scheme I), determined from the data of Figures 3 and 5. From the hyperbolic dependence of $1/\tau_1$ on IACoA concentration, we have obtained the magnitudes of $1/\tau_{1(max)}$, $1/\tau_{1(min)}$, and $K_{0.5}$ equal to 4.38 $s^{-1}$, 0.02 $s^{-1}$, and 14.5 $\mu$M, respectively.

*Interaction between MCAD–$FADH_2$ and IPCoA.* Having surmised that the substrate IPCoA enters into the reaction scheme for a second time, we suspected that IPCoA might have an affinity for the MCAD–$FADH_2$ form of the enzyme comparable to that for the MCAD–FAD enzyme form. To probe this, we attempted to detect a signal for the interaction between MCAD–$FADH_2$ (generated upon reduction of MCAD–FAD by sodium dithionite) and IPCoA by UV/vis, fluorescence, and CD spectroscopic techniques. While the former two techniques failed to show any meaningful interactions, a weak signal for the interaction was detected by CD spectroscopy. Figure 8 shows the CD spectra of sodium dithionite-reduced MCAD–FAD in the absence and in the presence of IPCoA under anaerobic conditions. Note that in the presence of IPCoA the 395-nm negative peak is shifted to 408 nm, giving a maximum change in ellipticity at 420 nm. However, the signal for interaction was so weak that we could not use a conventional titration method to determine the dissociation constant for the MCAD–$FADH_2$–IPCoA complex. Recourse was made to the titration strategy and data analysis developed in this laboratory (Wang et al., 1992). The Figure 8 inset shows the results of titrating MCAD–$FADH_2$ with increasing volumes of a fixed concentration of IPCoA. Analysis of the experimental results gives an observed dissociation constant of 0.3 $\mu$M.

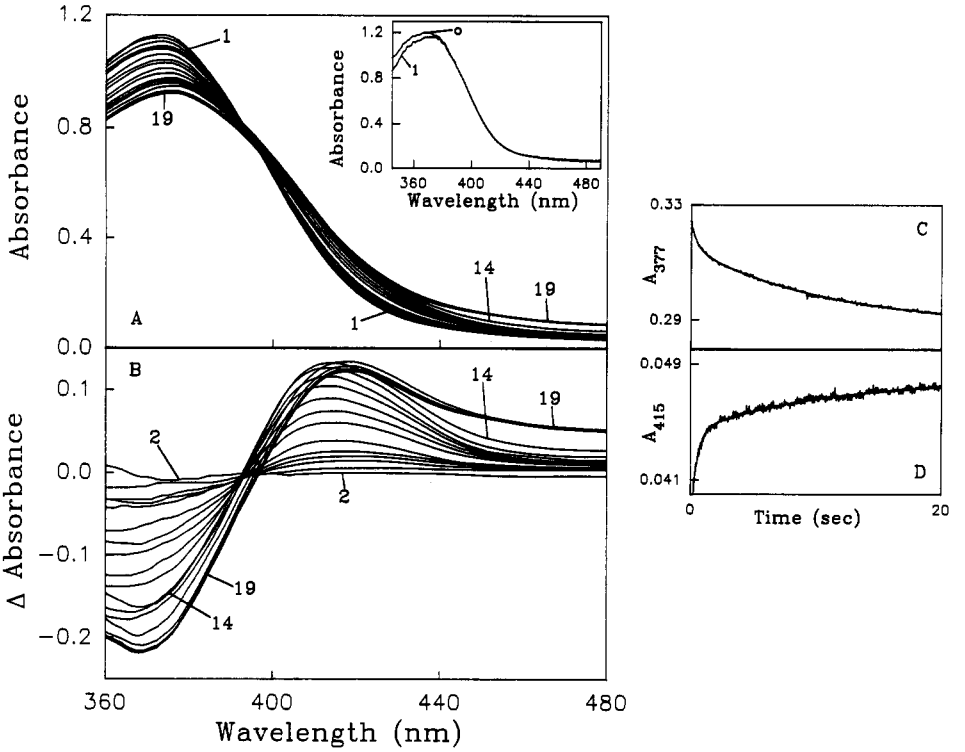


FIGURE 6: Rapid-scanning stopped-flow (panels A and B) and single-wavelength stopped-flow (panels C and D) data for the oxidation of MCAD–$FADH_2$ by IACoA. For RSSF experiments, 20 $\mu$M MCAD–$FADH_2$ was mixed with 50 $\mu$M IACoA in the stopped-flow syringes at zero time, and the spectra were collected at the following times after the first scan: (2) 0.0086, (3) 0.026, (4) 0.043, (5) 0.052, (6) 0.06, (7) 0.069, (8) 0.138, (9) 0.224, (10) 0.31, (11) 0.48 ,(12) 0.65, (13) 1.08, (14) 4.1, (15) 10.2, (16) 51.5, (17) 206, (18) 258, and (19) 282 s. The inset in panel A shows a comparison of the zero-time spectrum (reconstituted by summation of the individual spectra of IACoA and MCAD–$FADH_2$, obtained upon mixing of the individual species against the standard buffer in the stopped-flow syringes) and the first spectrum (collected within 1–2 ms after mixing). Spectra in panel B represent the difference spectra derived from the data of panel A. Other conditions are the same as in Figure 2. Panels C and D show the time courses for the stopped-flow MCAD–$FADH_2$ + IACoA reaction at 377 and 415 nm, respectively. The concentration of MCAD–$FADH_2$ and IACoA (before mixing) were 2 and 15 $\mu$M, respectively. Solid lines in panels C and D represent the best fits of the experimental data according to a double exponential rate equation. The relaxation rate constants derived from this analysis were found to be as follows: for panel C, $1/\tau_1 = 2.05\ s^{-1}$, $1/\tau_2 = 0.1\ s^{-1}$ at 377 nm; and for panel D, $1/\tau_1 = 2.1\ s^{-1}$, $1/\tau_2 = 0.1\ s^{-1}$ at 415 nm.

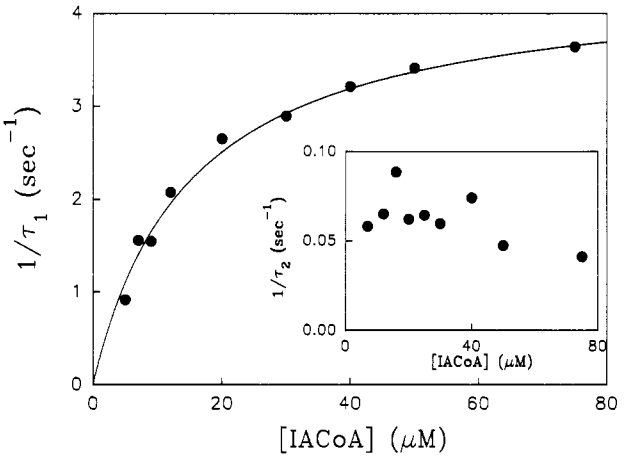


FIGURE 7: IACoA concentration-dependent relaxation rate constants ($1/\tau_1$ and $1/\tau_2$) for the reaction of MCAD–$FADH_2$ and IACoA, calculated from the reaction traces at 415 nm. The enzyme concentration was 1 $\mu$M after mixing. The $x$-axis represents the IACoA concentration after mixing. Other conditions are the same as in Figure 2. The solid line has been calculated for a hyperbolic dependence (with an offset) of $1/\tau_1$ as a function of IACoA concentration with $1/\tau_{1(max)}$, $1/\tau_{1(min)}$, and $K_{0.5}$ equal to 4.38 $s^{-1}$, 0.02 $s^{-1}$, and 14.9 $\mu$M, respectively. The inset shows the dependence of $1/\tau_2$ on IACoA concentration.

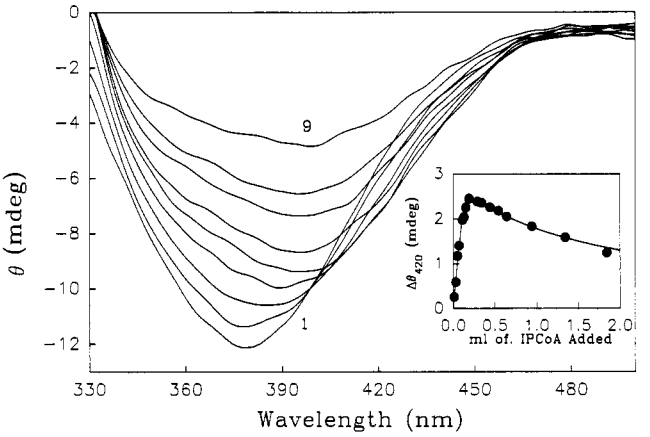


FIGURE 8: Circular dichroic spectra for the interaction of MCAD–$FADH_2$ and IPCoA. A 1.65-mL volume of MCAD–$FADH_2$ (25 $\mu$M), reduced with sodium dithionite, was titrated with known volumes of a stock concentration of 0.2 mM IPCoA. The spectra shown are at the following concentrations of IPCoA: 0, 4.6, 10.4, 16, 26.5, 43.9, 71.8, 93.3, and 135 $\mu$M. Inset: the change in ellipticity ($\theta$) at 420 nm plotted as a function of volume of IPCoA added. The change in $\theta$ at 420 nm was calculated by subtracting the signal associated with reduced enzyme, corrected for dilution, from the signal of the reduced enzyme–IPCoA mixture. The solid line is the best fit of the data according to the equation of Wang et al. (1992), giving a dissociation constant for the MCAD–$FADH_2$–IPCoA complex of 0.3 $\mu$M.

## DISCUSSION

The experimental results presented in the previous section emphasize the advantage of using a chromophoric substrate, in conjunction with the RSSF method, for delineating the microscopic pathway of the MCAD-catalyzed reaction. The major outcome of our experimental design is the demonstration of a spectrally distinct intermediary species (absorption

maximum = 400 nm) during the course of MCAD catalysis. The fact that this species is formed only when IPCoA is utilized as the enzyme substrate and not when butyryl-CoA is utilized as the substrate (Pohl et al, 1986; also our unpublished results) suggests that the intermediary spectral band is primarily contributed by the electronic structure of the reaction product IACoA. Furthermore, the substrate-specific origin of the new spectral band eliminates the possibility that it is caused by the formation of a metastable blue semiquinone species, a species that is formed during anaerobic titration of the enzyme with dithionite (Thorpe et al., 1979).

A close examination of the time-resolved spectra, in both the forward and reverse directions, of the MCAD reaction, vis-à-vis the spectra of the individual chromophoric species (see Figure 1), reveals the following features. (1) The intermediary spectral band is formed in the enzyme-catalyzed reaction both in the forward and reverse directions. (2) In the forward direction, the formation of the intermediary spectral band (located at 400 nm) accompanies the reduction of the enzyme-bound flavin moiety, as evidenced by the decrease in the major flavin absorption peak at 450 nm. (3) The formation of the intermediary species (in the forward direction) is also accompanied by the appearance of a broad charge-transfer band at 600 nm. Such charge-transfer bands have been observed for most of the enzyme substrates, albeit at different absorption maxima (Murfin, 1974; Reinsch et al., 1980). (4) Under conditions where [MCAD–FAD] >> [IPCoA], both the intermediary spectral band (400 nm) and the charge-transfer band (600 nm) remain stable, whereas when [MCAD–FAD] << [IPCoA], both of these spectral bands slowly collapse. The 400-nm band slowly shifts to the spectral band, which is more characteristic of a mixture of aqueous IACoA and MCAD–$FADH_2$-bound IACoA (absorption maximum = 373 nm), while the charge-transfer band simply decreases in magnitude. The time courses of spectral changes (at 400- and 600-nm regions) are remarkably similar, irrespective of the relative concentrations of [MCAD–FAD] and [IPCoA]. (5) A slight red shift in the IACoA spectrum is observed upon the interaction of IACoA with MCAD–$FADH_2$ within the dead time of our stopped-flow.

In the light of these time-resolved spectral characteristics, it is obvious that the enzyme-bound intermediate, which is responsible for the 400-nm spectral band, gives rise also to the charge-transfer band, and both of these bands are given by the reduced form of the enzyme (i.e., MCAD–$FADH_2$). The question arises as to the chemical nature of this intermediate.

Given that the electronic spectrum of IACoA is red-shifted upon interaction with either the oxidized or reduced forms of the enzyme, it may appear, intuitively, that the 400-nm spectral band is simply caused by polarization of the carbonyl group of IACoA within the enzyme site phase (Johnson et al., 1992). However, under no static experimental conditions (viz. extremes of pH, different redox states of the enzyme, etc.) did we observe such a large spectral shift in the IACoA absorption maximum, i.e., from 367 nm in the aqueous solution to 400 nm in the enzyme site phase. Hence, it appears likely that such an extensive red shift in the electronic structure of IACoA is caused by the conjugation of the $\pi$-electrons of the IACoA moiety with those of the reduced flavin ring. This, coupled with the fact that the same (chromophoric) intermediary species is also responsible for producing the charge-transfer band, attests to its specialized structural feature. An explicit chemical nature of this intermediate must await X-ray crystallographic determinations of the enzyme–intermediate complex to atomic resolutions.

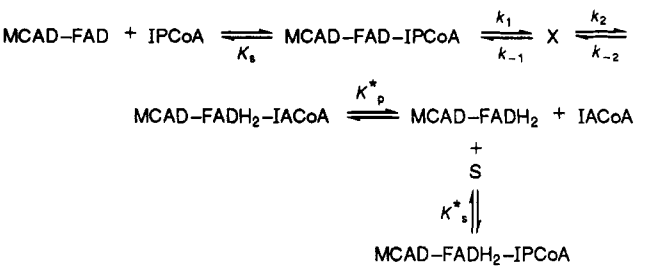


The postulation that the intermediate formed during the MCAD-catalyzed reaction is specialized in nature is not novel to this investigation. Several earlier investigators have arrived at the same conclusion on the basis of circumstantial evidence (Ikeda et al., 1985; Schopfer et al., 1988). However, of these, the proposition that the intermediate is a resonance hybrid involving oxidized flavin, an acyl-CoA carbanion, and a mutually shared hydride ion (Ikeda et al., 1985) does not seem to be supported by our RSSF data. Our RSSF data clearly suggest that the intermediate possesses the properties of reduced flavin and the oxidized substrate, albeit the latter appears to be highly conjugated.

The fact that there are no spectral changes (particularly around the 450-nm region) within the dead time of our stopped flow (3–5 ms) during the MCAD–FAD + IPCoA reaction, suggests that the electronic spectrum of the flavin remains unperturbed within the dead time of the stopped flow. This observation is slightly contradictory to the results of Pohl et al. (1986), who showed that perdeuteriobutyryl-CoA perturbs the electronic structure of the enzyme-bound flavin within the Michaelian complex. We offer no explanation for this discrepancy. However, when we performed the RSSF studies for the reaction of MCAD–$FADH_2$ with IACoA, we observed a small red shift of the IACoA spectrum (within the dead time of our stopped flow), suggesting that a small electronic structural change in IACoA takes place even in the Michaelian complex. A large change in the electronic structure of IACoA, however, takes place upon the slow isomerization of the MCAD–$FADH_2$–IACoA complex.

The results of the transient kinetic analysis for the dehydrogenase half-reaction showed a process consistent with one ($1/\tau$) and two relaxations steps ($1/\tau_1 >> 1/\tau_2$) under conditions of high and low enzyme concentration, respectively. The fact that $1/\tau_2$ appears only when [IPCoA] >> [MCAD–FAD] but not when [MCAD–FAD] >> [IPCoA] attests to the entrance of IPCoA in the reaction pathway for a second time (Schopfer et al., 1988). Furthermore, when $1/\tau_1$ was analyzed as a function of [IPCoA], it was found that $1/\tau_{1(min)}$, $1/\tau_{1(max)}$, and $K_{0.5}$ values were remarkably similar to the corresponding values obtained upon analyzing the data for $1/\tau$ versus [MCAD–FAD] (under conditions where [MCAD–FAD] >> [IPCoA]). These facts suggest that the events occurring during $1/\tau_1$ precede those occurring during $1/\tau_2$, whereby the intermediary chromophoric species (i.e., X) builds up during the first phase, and its disappearance takes place in the second phase of the reaction. A cumulative account of all the experimental results leads us to propose a minimal kinetic model for the MCAD-catalyzed reaction under conditions where [IPCoA] >> [MCAD–FAD] (Scheme I). This scheme is similar to that proposed by Schopfer et al. (1988) for the MCAD-catalyzed reaction utilizing butyryl/crotonyl-CoA as the substrate/product pair, respectively. The entrance of IPCoA into the reaction scheme for the second time is directly supported by the demonstration of its interaction with the reduced form of the enzyme ($K_d$ = 0.3

$\mu$M). This $K_d$ is qualitatively similar to the $K_d$ of $7 \times 10^{-8}$ M for the MCAD–$FADH_2$–butyryl-CoA complex (Schopfer et al., 1988).

On the basis of the $k_{cat}$ and $K_m$ for the enzyme-catalyzed reaction involving IPCoA as a substrate (Johnson et al., 1992), it can be argued that the MCAD-catalyzed reaction conforms to a rapid equilibrium condition (Fersht, 1985). Hence, the enzyme substrate/product equilibration reactions can be taken to be much faster than the chemical transformation steps. This provision simplifies the kinetic model of Scheme I to the following form:

$$MCAD_{ox} \underset{k_{-1}}{\overset{\alpha}{\rightleftharpoons}} X \underset{\beta}{\overset{k_2}{\rightleftharpoons}} MCAD_{red} \quad (2)$$

where $MCAD_{ox}$ = MCAD–FAD + MCAD–FAD–IPCoA and $MCAD_{red}$ = MCAD–$FADH_2$ + MCAD–$FADH_2$–IACoA + MCAD–$FADH_2$–IPCoA, $\alpha$ and $\beta$ are the cumulative aggregates of the rate and equilibrium constants as given by:

$$\alpha = \frac{k_1[\text{IPCoA}]}{[\text{IPCoA}] + K_s} \quad (3)$$

$$\beta = \frac{k_{-2}}{1 + (K^*_p/[\text{IACoA}])(1 + ([\text{IPCoA}]/K^*_s))} \quad (4)$$

The two (slow)-step equilibration reaction of eq 2 predicts two relaxation times (i.e., $\tau_1$ and $\tau_2$), as has been observed experimentally. Without making any assumptions, the relaxation rate constants ($1/\tau$ values) are related by the forward and reverse rate constants of eq 2, i.e., $\alpha$, $k_{-1}$, $k_2$, and $\beta$, by eqs 5 and 6 (Bernasconi, 1976).

$$1/\tau_1 + 1/\tau_2 = \alpha + k_{-1} + \beta + k_2 \quad (5)$$

$$(1/\tau_1)(1/\tau_2) = \alpha k_2 + \alpha\beta + k_{-1}\beta \quad (6)$$

On cursory examination of the dependence of $\alpha$ on IPCoA concentrations (eq 3), it occurred to us, on first sight, that the individual rate constants of Scheme I could be obtained from the above relationships between $1/\tau_1 + 1/\tau_2$ and [IPCoA] and between $(1/\tau_1)(1/\tau_2)$ and [IPCoA]. But we soon realized that since $\beta$ is dependent not only on [IPCoA] but also on the IACoA concentration (which in turn is also a function of the IPCoA concentration), no analytical solutions of our experimental results (based on eqs 5 and 6) could be obtained. In situations of this kind, recourse is often made to simulating the experimental results by numerical methods (Srivastava et al., 1989). Before undertaking the latter step, we first explored the possibility of obtaining the individual rate constants of Scheme I by some alternative methods. In this effort, we noticed that the magnitudes of the $1/\tau$ values for reactions in either direction (at saturating concentrations of substrates) differ at least by a factor of 40, suggesting that the equilibration rates intrinsic to the individual relaxation steps are not comparable. In this situation, the mutual coupling between two relaxation steps can be taken to be weak, and thus the relationships given by eqs 5 and 6 can be considerably simplified. For $1/\tau_1 >> 1/\tau_2$, $1/\tau_1$ can be taken to be a measure of $\alpha + k_{-1}$ (for the reaction in the forward direction), and thus $1/\tau_{(max)}$, $1/\tau_{(min)}$, and $K_{0.5}$, obtained from the data of Figure 5, will correspond to $k_1 + k_{-1}$ (0.63 $s^{-1}$), $k_{-1}$ (0.1 $s^{-1}$), and $K_s$ (9.0 $\mu$M) respectively. From these results, $k_1$ was calculated to be 0.53 $s^{-1}$.

The lack of a strong mutual coupling between the two relaxation steps (in the forward direction) is further illustrated by the fact that the dependence of $1/\tau$ on [MCAD] (the condition where a single relaxation is observed, Figure 3) yields remarkably corresponding values of $1/\tau_{(max)}$, $1/\tau_{(min)}$, and $K_{0.5}$ (see Results). Thus, taking $1/\tau = \alpha + k_{-1}$, the magnitudes of $k_1$, $k_{-1}$, and $K_{0.5}$ can be calculated to be 0.62 $s^{-1}$, 0.08 $s^{-1}$, and 14 $\mu$M, respectively. An average value of these parameters from the data of Figures 3 and 5 is given in Table I. It is apparent from the relationship between $\beta$ and [IPCoA] that as [IPCoA] approaches infinity, $\beta$ becomes negligible, and thus the slower relaxation rate constant ($1/\tau_2$) is dominated by $k_2$ (i.e., the forward rate constant for the conversion of X to MCAD–$FADH_2$–IACoA). This is what is often referred to as the quasi-irreversible condition (MacGibbon et al., 1987) and is supported by the attainment of a horizontal asymptote on the $1/\tau_2$ versus [IPCoA] plot.

Table I: Microscopic Parameters for the Model Proposed in Scheme I

| parameter | experimentally determined | used in simulation |
|---|---|---|
| $K_s$ | 11.5 $\mu$M | 10 $\mu$M |
| $k_1$ | 0.57 $s^{-1}$ | 0.4 $s^{-1}$ |
| $k_{-1}$ | 0.09 $s^{-1}$ | 0.15 $s^{-1}$ |
| $k_2$ | 0.01 $s^{-1}$ | 0.01 $s^{-1}$ |
| $k_{-2}$ | 4.36 $s^{-1}$ | 4.0 $s^{-1}$ |
| $K^*_p$ | 14.5 $\mu$M | 10.0 $\mu$M |
| $K^*_s$ | 0.3 $\mu$M | 0.3 $\mu$M |

The remaining microscopic parameters of Scheme I were obtained from the transient kinetic results for the enzyme-catalyzed reaction in the reverse direction. As in the forward direction, the reverse reaction (under conditions [IACoA] >> [MCAD–$FADH_2$]) is also consistent with two relaxation times. Since $1/\tau_1$ is at least 40 times higher than $1/\tau_2$, according to the discussion presented above these two relaxation times can be treated as uncoupled. Hence, for the rapid equilibrium condition, $1/\tau_1$ can be given in terms of the following microscopic parameters of Scheme I:

$$\frac{1}{\tau_1} = k_2 + \frac{k_{-2}}{1 + (K^*_p/[\text{IACoA}])} \quad (7)$$

Consistent with this equation, $1/\tau_{(max)}$, $1/\tau_{(min)}$, and $K_{0.5}$ (obtained from the data of Figure 7) correspond to $k_2 + k_{-2}$ (4.38 $s^{-1}$), $k_{-2}$ (0.02 $s^{-1}$), and $K^*_p$ (14.5 $\mu$M), respectively. From these data, $k_2$ was calculated to be 4.36 $s^{-1}$. These values are given in Table I. Note that the magnitude of $k_2$ obtained from this result is remarkably similar to that obtained from the data of Figure 5. At this point, we have not rigorously analyzed the dependence of $1/\tau_2$ on IACoA concentration. However, we do notice that at a saturating concentration of IACoA, the relaxation rate constant $1/\tau_2$ is similar to $k_{-1}$ (i.e., the reverse rate constant for the breakdown of X to MCAD–FAD–IPCoA complex).

Given all the microscopic parameters obtained for the kinetic model of Scheme I, we proceeded to simulate the time-dependent appearances of different species (of Scheme I) during the reaction progress in the forward direction by numerical methods (see Materials and Methods). The association ("on") rate constants for all enzyme substrate/product species have been taken be equal to $1 \times 10^8$ $M^{-1}$ $s^{-1}$ (the diffusion-limited rate constant; Hammes, 1982). The dissociation ("off") rate constant has been calculated from the equilibrium constant and the "on" rate constant by the relationship $k_{off} = k_{on}K_{eq}$. Figure 9 shows several simulated curves for the time-dependent appearance/disappearance of MCAD–FAD–IPCoA, X, and IACoA under diverse experimental conditions. Note that under conditions when [MCAD–

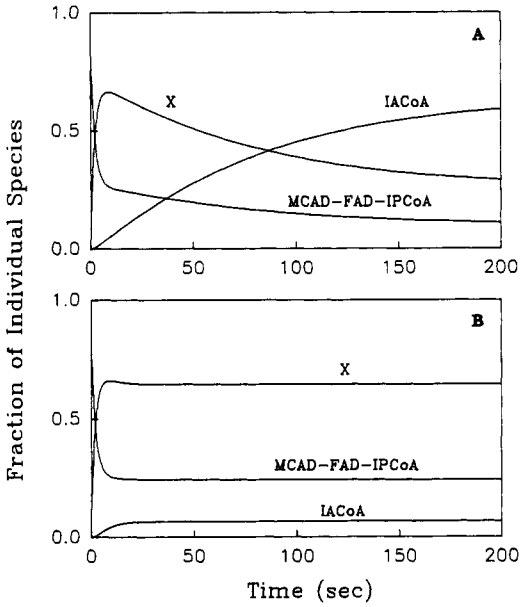


FIGURE 9: Computer simulation results for the MCAD–FAD + IPCoA reactions for the kinetic model of Scheme I. The time courses for the appearance of MCAD–FAD–IPCoA, X, and IACoA species under reaction conditions [IPCoA] >> [MCAD–FAD] (panel A) and [MCAD–FAD] >> IPCoA (panel B) have been calculated on the basis of the microscopic parameters listed in Table I. The concentrations of MCAD–FAD and IPCoA have been assumed to be as follows for the simulated curves: for panel A, [MCAD–FAD] = 5 $\mu$M, [IPCoA] = 100 $\mu$M; and for panel B, [MCAD–FAD] = 100 $\mu$M, [IPCoA] = 5 $\mu$M. Note that the time course for the appearance of all the species in panel A ([IPCoA] >> [MCAD–FAD]) exhibits biphasic characteristics, whereas the time course for the appearance of the same species in panel B ([MCAD–FAD] >> [IPCoA]) exhibits single exponential characteristics. The relaxation rate constants calculated from the best fit of these results according to double (panel A) and single (panel B) exponential rate equations were found to be $1/\tau_1 = 0.51\ s^{-1}$, $1/\tau_2 = 0.019\ s^{-1}$, and $1/\tau = 0.5\ s^{-1}$. Note that these values are remarkably similar to those obtained from the data of Figures 2 and 4.

FAD] >> [IPCoA] X approaches a constant value at a saturating concentration of IPCoA, whereas when [IPCoA] >> [MCAD–FAD] the magnitude of X first increases with time, attains a maximum value, and then starts decreasing. The relaxation rate constants calculated from the best fit (by a two-exponential rate equation) of the simulated data of Figure 9A were found to be 0.51 and 0.019 $s^{-1}$, respectively. Note that these values are remarkably similar to those obtained from the experimental data of Figures 4 and 5. Similarly, the (single) relaxation rate constant calculated from the best fit (by a single exponential rate equation) for the simulated data of Figure 9B was found to be 0.5 $s^{-1}$. Note a remarkable similarity between this value and that obtained from the experimental results of Figures 2 and 3. These similarities attest to the internal consistency of our kinetic model.

IACoA interacts with the oxidized form of the enzyme with a $K_d$ of 2.7 $\mu$M for the MCAD–FAD–IACoA complex (our unpublished results). This value is comparable to the binding constant for the MCAD–$FADH_2$–IPCoA complex reported here (see Table I). Thus, under experimental conditions where [MCAD–FAD] >> [IPCoA], the free IACoA formed during the reaction progress is likely to combine with the unreacted enzyme species (i.e., MCAD–FAD). This would result in the subsequent disappearance of X (as in case when [IPCoA] >> [MCAD–FAD]) and would thus give at least two relaxation times. This expectation is absolutely contrary to our experimental observations. The only explanation we can offer at this time against this expectation is that IACoA does not dissociate from the MCAD–$FADH_2$ form of the enzyme unless IPCoA enters into the reaction scheme for a second time. We are currently examining this latter possibility and will report our findings subsequently.

A close look at of the kinetic model of Scheme I, vis-à-vis the MCAD–FAD–IACoA binding results (Johnson et al., 1992), provides some interesting correlations regarding structural–functional relationships in enzyme catalysis. The facts that the interaction of MCAD–FAD and IACoA proceeds in two steps and that the second step involves obligatory changes in the protein conformation (Johnson et al., 1992) is qualitatively analogous to what is observed during catalysis. In the forward reaction, the colored intermediate (absorption maximum = 400 nm) follows the formation of the MCAD–FAD–IPCoA Michaelian complex. Since the electronic structure of IACoA is perturbed within this intermediate, it is likely that complementary protein conformational changes must have occurred to stabilize this species. The only difference between these two processes is that in the latter case the protein conformational changes have been coupled to "chemistry" (besides stabilizing alternative ligand structure), whereas in the former case the protein conformational changes just stabilize an electronically perturbed ligand species. Interestingly, the binding constants for the Michaelian complexes in both of these situations are approximately 10 $\mu$M. A similar analogy can be found for the MCAD–$FADH_2$ + IACoA reaction. This reaction also proceeds in two steps. The first step involves the formation of an MCAD–$FADH_2$–IACoA Michaelian complex, which undergoes chemical transformation, once again coupled with protein conformational changes (so as to stabilize the newly formed electronically distinct intermediary species). The dissociation constant for this Michaelian complex is also approximately 10 $\mu$M. Given this consistency, it is tempting to speculate that the binding of MCAD–$FADH_2$ with IPCoA is also a two-step process.

A comparison of the kinetic constants of Scheme I with the steady state turnover of the enzyme-catalyzed dehydrogenation and oxidation reaction reveals some interesting correlations. The apparent $k_{cat}$ for the dehydrogenation reaction (0.46 $s^{-1}$) precisely matches the forward rate constant for the formation of the intermediary species, whereas the apparent $k_{cat}$ for the oxidation reaction (0.016 $s^{-1}$) matches the forward rate constant for the disappearance of the intermediate X (Johnson et al., 1992). This clearly suggests that the rate-limiting step of the dehydrogenation reaction is the formation of X, whereas the rate-limiting step for the oxidation reaction is the disappearance of X (using IPCoA as the substrate). This also provides a qualitative explanation for the apparent $K_m$ for IPCoA in the oxidation reaction (0.49 $\mu$M) being lower than that obtained for the dehydrogenation reaction [10.3 $\mu$M (Johnson et al., 1992)]. We are currently in the process of elaborating on the microscopic pathways of the dehydrogenation and oxidation reactions, and we will report on these findings subsequently.

## ACKNOWLEDGMENT

We are thankful to Dr. Michael F. Dunn, Riverside, CA, for providing his technical expertise during the initial setup of our rapid scanning system and to Dr. Zhi-Xin Wang for stimulating discussions.

## REFERENCES

Auer, H. E., & Frerman, F. E. (1980) *J. Biol. Chem. 255*, 8157–8163.

Beinert, H. (1963) in *The Enzymes* (Boyer, P. D., Lardy, H., & Myrbach, K., Eds.) Vol. 7, pp 447–473, Academic Press, New York.
Bernasconi, C. F. (1976) in *Relaxation Kinetics*, Academic Press, New York.
Betts, G. F., & Srivastava, D. K. (1991) *J. Theor. Biol. 151*, 155–167.
Crane, F. L., & Beinert, H. (1956) *J. Biol. Chem. 219*, 717–731.
Crane, F. L., Mii, S., Hauge, J. G., Green, D. E., & Beinert, H. (1956) *J. Biol. Chem. 218*, 701–716.
Engel, P. C. (1992) in *Chemistry and Biochemistry of Flavoenzymes* (Muller, F., Ed.) Vol. III, pp 597–655, CRC Press, Inc., London.
Fersht, A. (1985) in *Enzyme Structure and Mechanism,* 2nd Ed., W. H. Freeman and Co., New York.
Ghisla, S., Thorpe, C., & Massey, V. (1984) *Biochemistry 23*, 3154–33161.
Hall, C. L., Lambeth, J. D., & Kamin, H. (1979) *J. Biol. Chem. 254*, 2023–2031.
Hammes, G. G. (1982) in *Enzyme Catalysis and Regulation*, Academic Press, New York.
Ikeda, Y., Hine, D. G., Okamura-Ikeda, K., & Tanaka, K. (1985) *J. Biol. Chem. 260*, 1326–1337.
Johnson, J. K., Wang, Z., & Srivastava, D. K. (1992) *Biochemistry 31*, 10564–10575.
Knoop, F. (1904) *Beitr. Chem. Physiol. Pathol. 6*, 150.
Koerber, S. C., MacGibbon, A. K. H., Dietrich, H., Zeppezauer, M., & Dunn, M. F. (1983) *Biochemistry 22*, 3424–3431.
Lehman, T. C., Hale, D. E., Bhala, A., & Thorpe, C. (1990) *Anal. Biochem. 186*, 280–284.
MacGibbon, A. K. H., Koerber, S. C., Pease, K., & Dunn, M. F. (1987) *Biochemistry 26*, 3058–3067.
McFarland, J. T., Lee, M., Reinsch, J., & Raven, W. (1982) *Biochemistry 21*, 1224–1229.
Murfin, W. (1974) *Ph.D. Dissertation*, Washington University.
Pohl, B., Raichle, T., & Ghisla, S. (1986) *Eur. J. Biochem. 160*, 109–115.
Reinsch, J., Katz, A., Wean, J., Aprahamian, G., & McFarland, J. T. (1980) *J. Biol. Chem. 255*, 9093–9097.
Savitzsky, A., & Golay, M. J. E. (1964) *Anal. Chem. 36*, 1627–1639.
Schopfer, L. M., Massey, V., Ghisla, S., & Thorpe, M. (1988) *Biochemistry 27*, 6599–6611.
Srivastava, D. K., Smolen, P., Betts, G. F., Fukushima, T., Spivey, H. O., & Bernhard, S. A. (1989) *Proc. Natl. Acad. Sci. U.S.A. 86*, 6464–6468.
Thorpe, C., Matthews, R. G., & Williams, C. H., Jr. (1979) *Biochemistry 18*, 331–337.
Wang, Z., Kumar, N. R., & Srivastava, D. K. (1992) *Anal. Biochem. 206*, 376–381.